Acta Cryst E CRYSTALLOGRAPHIC COMMUNICATIONS
ISSN 2056-9890

Crystal structure of bis{3-(3,4-dimethylphenyl)-5-[6-(1*H*-pyrazol-1-yl)pyridin-2-yl]-4*H*-1,2,4-triazol-4-ido}iron(II) methanol disolvate

Kateryna Znovjyak,[a] Igor O. Fritsky,[a] Tatiana Y. Sliva,[a] Vladimir M. Amirkhanov,[a] Sergey O. Malinkin,[a] Sergiu Shova[b] and Maksym Seredyuk[a]*

[a]Department of Chemistry, Taras Shevchenko National University of Kyiv, Volodymyrska Street 64, Kyiv, 01601, Ukraine, and [b]Department of Inorganic Polymers, "Petru Poni", Institute of Macromolecular Chemistry, Romanian Academy of Science, Aleea Grigore Ghica Voda 41-A, Iasi 700487, Romania. *Correspondence e-mail: mlseredyuk@gmail.com

Received 31 August 2022
Accepted 4 October 2022

Edited by C. Schulzke, Universität Greifswald, Germany

Keywords: crystal structure; spin-crossover; spin transition; energy frameworks.

CCDC reference: 2211089

Supporting information: this article has supporting information at journals.iucr.org/e

As a result of the high symmetry of the *Aea*2 structure, the asymmetric unit of the title compound, $[Fe^{II}(C_{18}H_{15}N_6)_2]\cdot 2MeOH$, consists of half of a charge-neutral complex molecule and a discrete methanol molecule. The planar anionic tridentate ligand 2-[5-(3,4-dimethylphenyl)-4*H*-1,2,4-triazol-3-ato]-6-(1*H*-pyrazol-1-yl)pyridine coordinates the Fe^{II} ion meridionally through the N atoms of the pyrazole, pyridine and triazole groups, forming a pseudo-octahedral coordination sphere of the central ion. The average Fe—N bond distance is 1.955 Å, indicating a low-spin state of the Fe^{II} ion. Neighbouring cone-shaped molecules, nested into each other, are linked through double weak C—H(pz)···π(ph') interactions into mono-periodic columns, which are further linked through weak C—H···N′/C′ interactions into di-periodic layers. No interactions shorter than the sum of the van der Waals radii of the neighbouring layers are observed. Energy framework analysis at the B3LYP/6–31 G(d,p) theory level, performed to quantify the intermolecular interaction energies, reproduces the weak interlayer interactions in contrast to the strong interaction within the layers. Intermolecular contacts were quantified using Hirshfeld surface analysis and two-dimensional fingerprint plots, showing the relative contributions of the contacts to the crystal packing to be H···H 48.5%, H···C/C···H 28.9%, H···N/N···H 16.2% and C···C 2.4%.

1. Chemical context

Bisazolepyridines are a broad class of meridional tridentate ligands used to synthesize charged Fe^{II} compounds capable of switching between a spin state with the $t_{2g}^4e_g^2$ configuration (high-spin, total spin S = 2) and a spin state with the $t_{2g}^6e_g^0$ configuration (low-spin, total spin S = 0) due to temperature variation, light irradiation or external pressure (Halcrow, 2014; Halcrow *et al.*, 2019). In the case of asymmetric ligand design, where one of the azole groups carries a hydrogen on the nitrogen heteroatom, it was shown that deprotonation can produce neutral complex species that can be high-spin (Schäfer *et al.*, 2013), low-spin (Shiga *et al.*, 2019) or exhibit temperature-induced transitions between the spin states of the central atom (Seredyuk *et al.*, 2014), depending on the ligand field strength. The substituents of ligands can also play an important role in behaviour of the solid samples, determining the way molecules interact with each other and, therefore, influencing the spin state adopted by the central atom. As we have recently shown, the dynamic rearrangement of the substituent groups can lead to an abnormally large hysteresis of the thermal high-spin transition due to the supramolecular

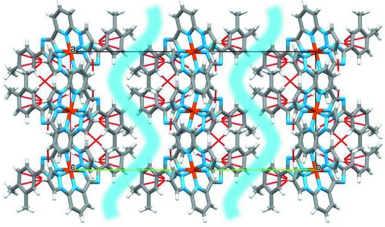

mechanism of blocking the deformation of the complex molecule by the methoxy group (Seredyuk *et al.*, 2022).

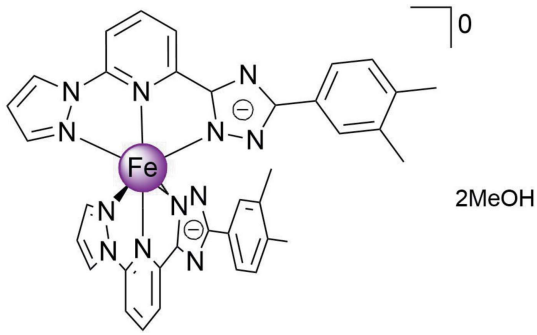

In a continuation of our interest in 3*d*-metal complexes formed by polydentate ligands (Bartual-Murgui *et al.*, 2017; Bonhommeau *et al.*, 2012; Valverde-Muñoz *et al.*, 2020), we report here the structural characterization of a new electroneutral complex $[Fe^{II}L_2]^0$ based on an asymmetric monodeprotonated ligand with two methyl substituents on the phenyl group, *L* = 2-[5-(3,4-dimethylphenyl)-4*H*-1,2,4-triazol-3-ato]-6-(1*H*-pyrazol-1-yl)pyridine.

2. Structural commentary

The asymmetric unit comprises half of the molecule and a discrete MeOH molecule forming a hydrogen bond O26—H26···N12 with the triazole (trz) ring (Fig. 1). The Fe^{II} ion has a pseudo-octahedral coordination environment composed of the nitrogen donor atoms of the pyrazole (pz), pyridine (py) and trz heterocycles with an average Fe—N distance of 1.957 Å (V[FeN$_6$] = 9.654 Å^3) being typical for low-spin complexes with an N_6 coordination environment (Gütlich & Goodwin, 2004). The pz, py, trz and phenyl rings, together with the two methyl substituents of one ligand, all lie essentially in the same plane.

The average trigonal distortion parameters, $\Sigma = \Sigma_1^{12}(|90 - \varphi_i|)$, with φ_i being the N—Fe—N′ angle (Drew *et al.*, 1995), and $\Theta = \Sigma_1^{24}(|60 - \theta_i|)$, with θ_i being the angle generated by superposition of two opposite faces of the octahedron (Chang *et al.*, 1990), are 92.8 and 295.0°, respectively. The values reveal a deviation of the coordination environment from an ideal octahedron which is, however, in the expected range for complexes with similar bisazolepyridine ligands (see below). The calculated continuous shape measure (CShM) value relative to the ideal O_h symmetry is 2.18 (Kershaw Cook *et al.*, 2015).

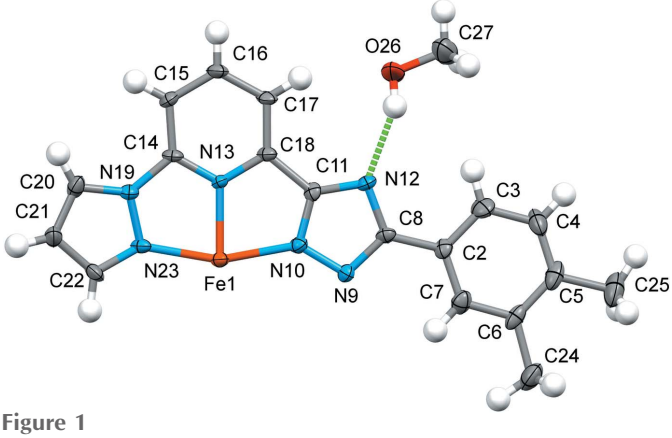

Figure 1
The molecular structure of half the title compound as refined in the asymmetric unit with displacement ellipsoids drawn at the 50% probability level. The O—H···N hydrogen bond is indicated by the dashed line. This and the next figure were generated with the program *Mercury* (Macrae *et al.*, 2020).

Table 1
Hydrogen bonding (Å) of the title compound.

Hydrogen bond	Length	Symmetry operation of the contact atom
C7···H—C21(pz)	2.827	$1 - x, 1 - y, 1 + z$
C6···H—C21(pz)	2.777	$1 - x, 1 - y, 1 + z$
C5···H—C21(pz)	2.756	$1 - x, 1 - y, 1 + z$
C4···H—C21(pz)	2.802	$1 - x, 1 - y, 1 + z$
C3···H—C21(pz)	2.893	$1 - x, 1 - y, 1 + z$
N9···H—C15(py)	2.475	$\frac{1}{2} + x, 1 - y, \frac{1}{2} + z$
N9···H—C20(pz)	2.522	$\frac{1}{2} + x, 1 - y, \frac{1}{2} + z$
H7···C20(pz)	2.641	$\frac{1}{2} + x, 1 - y, \frac{1}{2} + z$
N12···H—O26	2.017	x, y, z
H17···O26	2.329	x, y, z
O26···H—C22(pz)	2.257	$-\frac{1}{2} + x, 1 - y, \frac{1}{2} + z$

3. Supramolecular features

As a result of the tapered shape, neighbouring complex molecules are embedded in each other and interact through two weak intermolecular C—H(pz)···π(ph') contacts between the pyrazole (pz) and phenyl (ph) groups, respectively [distance C2)(pz)···C_g(ph') is 3.392 Å, angle between planes of the rings is 73.77°]. The formed mono-periodic supramolecular columns protrude along the *c*-axis with a stacking periodicity equal to 10.6511 (7) Å (= cell parameter *c*) (Fig. 2*a*). Weak intermolecular hydrogen-bonding interactions C—H(pz, py)···N/C(pz, trz)/O(MeOH) in the range 2.257–2.893 Å

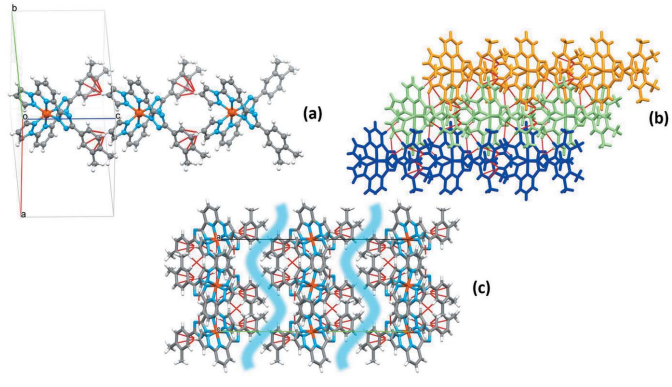

Figure 2
(*a*) A fragment of the mono-periodic supramolecular columns formed by stacking of molecules along the *c* axis. (*b*) Di-periodic supramolecular layers formed by stacking of the supramolecular columns. For a better representation, each column has a different colour. Red dashed lines represent weak hydrogen bonds. (*c*) Stacking of the di-periodic layers along the *c* axis. Blue shaded areas correspond to the interlayer space without intermolecular interactions shorter than the sum of the van der Waals radii. The methanol molecules are not shown for clarity.

(Table 1), link neighbouring columns into corrugated diperiodic layers in the *bc* plane (Fig. 2*b*,*c*). The layers stack along the *b*-axis direction without any strong or weak interlayer interactions shorter than the sum of the van der Waals radii (Fig. 2*c*). The voids between the layers are occupied by methanol molecules, which participate in the strong hydrogen bonding mentioned above, and weak hydrogen bonding with the aromatic substituents within the layers (a complete list of intermolecular interactions is given in Table 1).

4. Hirshfeld surface and 2D fingerprint plots

Hirshfeld surface analysis was performed and the associated two-dimensional fingerprint plots were generated using *Crystal Explorer* (Spackman *et al.*, 2021), with a standard resolution of the three-dimensional d_{norm} surfaces plotted over a fixed colour scale of −0.6122 (red) to 1.3609 (blue) a.u. (Fig. 3). The pale-red spots symbolize short contacts and negative d_{norm} values on the surface correspond to the interactions described above. The overall two-dimensional fingerprint plot is illustrated in Fig. 4. The Hirshfeld surfaces mapped over d_{norm} are shown for the H···H, H···C/C···H, H···N/N···H and C···C contacts, and the two-dimensional fingerprint plots, associated with their relative contributions to the Hirshfeld surface. At 48.5%, the largest contribution to the overall crystal packing is from H···H interactions, which are located mostly in the central region of the fingerprint plot. H···C/C···H contacts contribute 28.9%, resulting in a pair of characteristic wings. The H···N/N···H contacts, represented by a pair of sharp spikes in the fingerprint plot, make a 16.2%

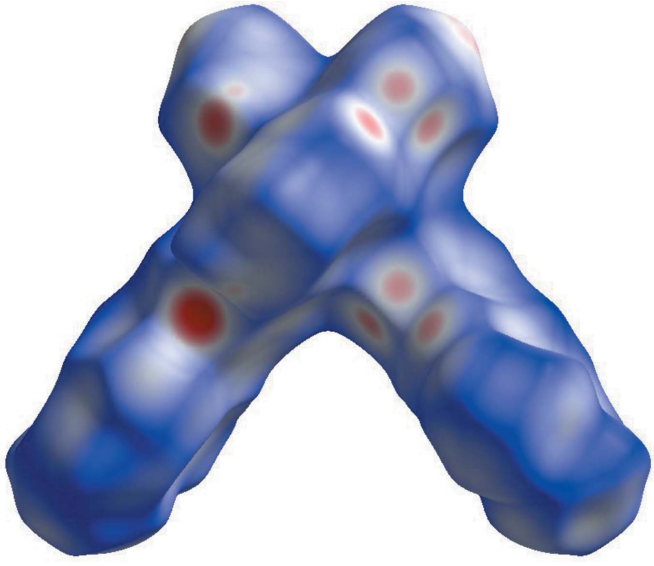

Figure 3
A projection of d_{norm} mapped on the Hirshfeld surface, showing the intermolecular interactions within the molecule. Red areas represent regions where contacts are shorter than the sum of the van der Waals radii, blue areas represent regions where contacts are longer than the sum of van der Waals radii, and white areas are regions where contacts are close to the sum of van der Waals radii. This and the next two figures were generated with the program *Crystal Explorer* (Spackman *et al.*, 2021).

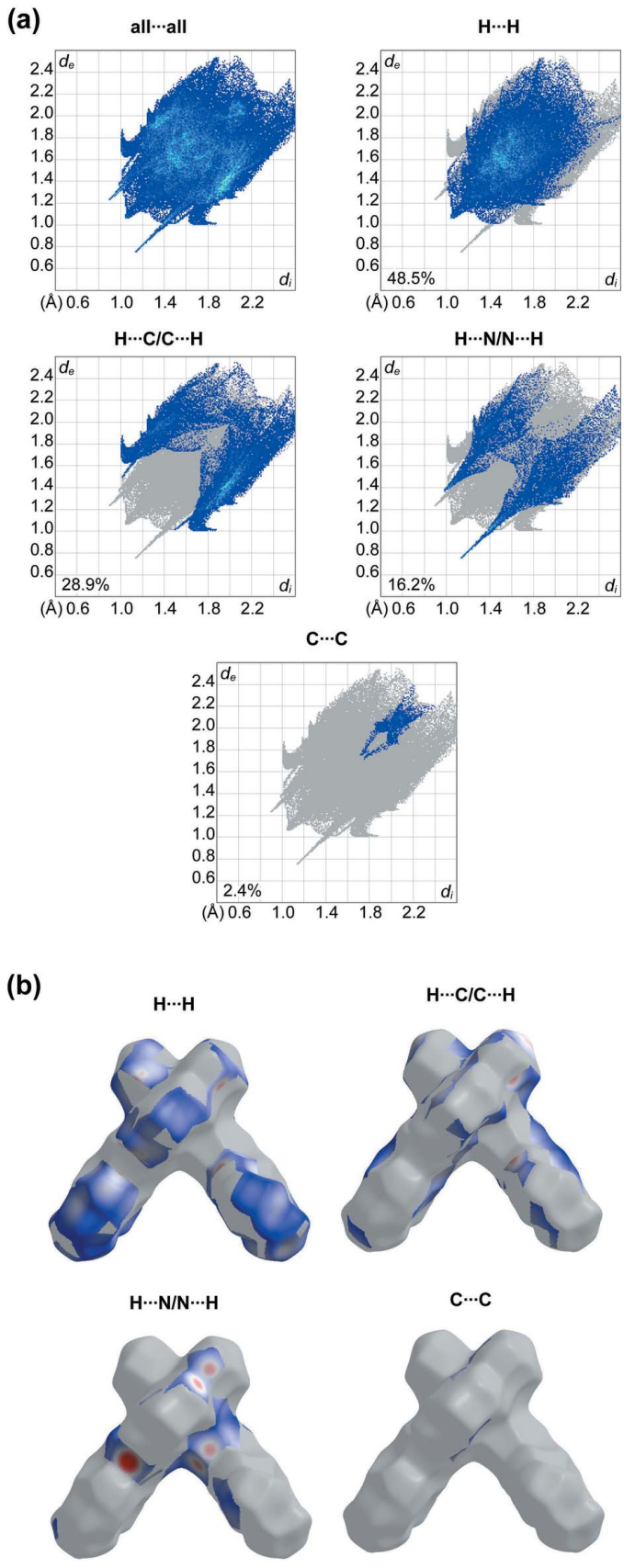

Figure 4
(*a*) The overall two-dimensional fingerprint plot and those decomposed into specified interactions. (*b*) Hirshfeld surface representations with the function d_{norm} plotted onto the surface for the different interactions.

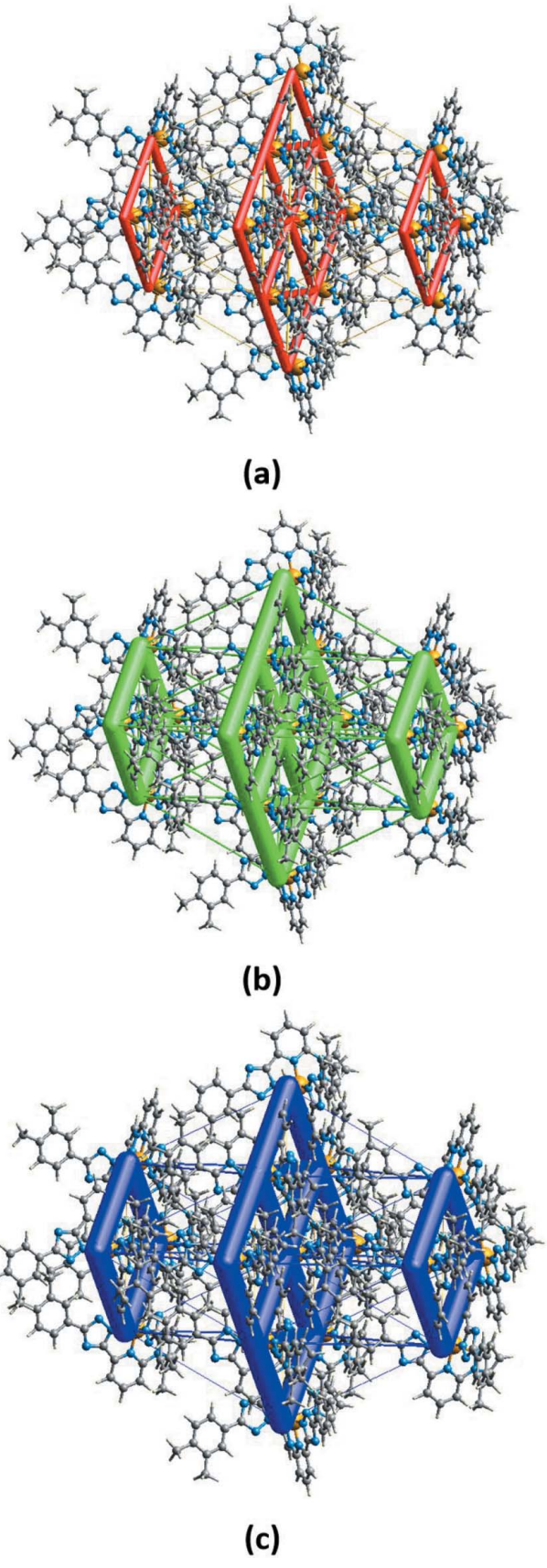

Figure 5
The calculated energy frameworks, showing (*a*) the electrostatic potential forces (E_{ele}), (*b*) the dispersion forces (E_{dis}) and (*c*) the total energy diagrams (E_{tot}). Tube size is set at 100 scale.

Table 2
Computed distortion indices (Å, °) for the title compound and similar literature complexes.

CSD code	Spin state	<Fe—N>	Σ	Θ	CShM(O_h)
Title compound	Low-spin	1.957	92.8	295.0	2.18
XODCEB[a]	Low-spin	1.950	87.4	276.6	1.92
QIDJET01[b]	Low-spin	1.970	90.3	341.3	2.47
QIDJET[b]	High-spin	2.184	145.5	553.3	5.88
DOMQIH[c]	Low-spin	1.962	83.8	280.7	2.02
DOMQUT[c]	Low-spin	1.991	88.5	320.0	2.48
DOMQUT02[c]	High-spin	2.183	139.6	486.9	5.31
EJQOA[d]	Low-spin	1.946	87.5	308.9	2.16
BEJQUG[d]	Low-spin	1.952	97.9	309.9	2.37
BEJQUG01[d]	High-spin	2.138	118.0	375.9	3.34
BEJRAN[d]	Low-spin	1.946	107.7	384.5	3.20
BEJRER[d]	High-spin	2.139	147.8	507.2	4.92

Notes: (*a*) Shiga *et al.* (2019); (*b*) Zhang *et al.* (2007); (*c*) Seredyuk *et al.* (2014); (*d*) Seredyuk *et al.* (2022).

contribution to the Hirshfeld surface. Finally, C···C contacts, which account for a contribution of 2.4%, are mostly distributed in the middle part of the plot.

5. Energy frameworks

The energy frameworks, calculated using the wave function at the B3LYP/6-31G(d,p) theory level, including the electrostatic potential forces (E_{ele}), the dispersion forces (E_{dis}) and the total energy diagrams (E_{tot}), are shown in Fig. 5 (Spackman *et al.*, 2021). The cylindrical radii, adjusted to the same scale factor of 100, are proportional to the relative strength of the corresponding energies. The major contribution to the intermolecular interactions comes from dispersion forces (E_{dis}), reflecting the dominant interactions in the network of the electroneutral molecules. The topology of the energy framework resembles the topology of the intermolecular interactions within and between the supramolecular layers described above. Because of the high lattice symmetry, there are only two different attractive interactions between the molecules within the layers, equal to −58.5 and −90.6 kJ mol^{-1}. As for the interlayer interactions, the absence of supramolecular bonding leads to very weak interactions in the range −7.4 to +2.5 kJ mol^{-1}, *i.e.* from weakly attracting to weakly repulsive. The colour-coded interaction mappings within a radius of 3.8 Å of a central reference molecule for the title compound together with full details of the various contributions to the total energy (E_{tot}) are given in the supporting information

6. Database survey

A search of the Cambridge Structural Database (CSD, Version 5.42, last update February 2021; Groom *et al.*, 2016) reveals several similar neutral Fe^{II} complexes with a deprotonated azole group, for example, those based on pyrazole-pyridine-benzimidazole, XODCEB (Shiga *et al.*, 2019), phenathroline-tetrazole, QIDJET (Zhang *et al.*, 2007), and phenanthroline-benzimidazole, DOMQUT (Seredyuk *et al.*, 2014). We also included in the comparison data for three

Table 3
Experimental details.

Crystal data	
Chemical formula	$[Fe(C_{18}H_{15}N_6)_2]\cdot 2CH_4O$
M_r	750.65
Crystal system, space group	Orthorhombic, *Aea*2
Temperature (K)	180
a, *b*, *c* (Å)	12.6854 (10), 26.315 (2), 10.6511 (7)
V (Å^3)	3555.5 (5)
Z	4
Radiation type	Mo *Kα*
μ (mm^{-1})	0.48
Crystal size (mm)	0.3 × 0.24 × 0.04
Data collection	
Diffractometer	Xcalibur, Eos
Absorption correction	Multi-scan (*CrysAlis PRO*; Rigaku OD, 2022)
T_{min}, T_{max}	0.824, 1.000
No. of measured, independent and observed [$I > 2\sigma(I)$] reflections	6911, 3047, 2211
R_{int}	0.071
(sin $\theta/\lambda)_{max}$ (Å^{-1})	0.595
Refinement	
$R[F^2 > 2\sigma(F^2)]$, $wR(F^2)$, *S*	0.061, 0.100, 1.00
No. of reflections	3047
No. of parameters	247
No. of restraints	1
H-atom treatment	H atoms treated by a mixture of independent and constrained refinement
$\Delta\rho_{max}$, $\Delta\rho_{min}$ (e Å^{-3})	0.84, −0.50
Absolute structure	Flack *x* determined using 703 quotients $[(I^+)-(I^-)]/[(I^+)+(I^-)]$ (Parsons *et al.*, 2013).
Absolute structure parameter	−0.02 (3)

Computer programs: *CrysAlis PRO* (Rigaku OD, 2022), *SHELXT* (Sheldrick, 2015*a*), *SHELXL2018/3* (Sheldrick, 2015*b*) and *OLEX2* (Dolomanov *et al.*, 2009).

polymorphs, in different spin states, of a complex structurally similar to the title compound, but carrying a methoxy group on the phenyl substituent (EJQOA, BEJQUG, BEJQUG01, BEJRAN, BEJRER; Seredyuk *et al.*, 2022) (see schematic structures of all complexes in the supporting information. The Fe—N distances of these complexes in the low-spin state are 1.946–1.991 Å, while in the high-spin state they are in the range 2.138–2.184 Å. The values of the trigonal distortion and CShM(O_h) change correspondingly, and in the low-spin state they are systematically lower than in the high-spin state. The respective structural parameters of the title compound and related complexes are given in Table 2.

7. Synthesis and crystallization

The ligand *L* was synthesized by the Suzuki cross-coupling reaction from the commercially available precursors (Enamine Ltd.) according to the method described in the literature (Seredyuk *et al.*, 2022). The synthesis of the title compound was performed with a layering technique in a standard test tube. The layering sequence was as follows: the bottom layer contained a solution of $[Fe(L_2)](BF_4)_2$ prepared by dissolving *L* = 2-[(3,4-dimethylphenyl)-4*H*-1,2,4-triazol-3-yl)]-6-(1*H*-pyrazol-1-yl)pyridine (100 mg, 0.316 mmol) and $Fe(BF_4)_2\cdot 6H_2O$ (53 mg, 0.158 mmol) in boiling acetone, to which chloroform (5 ml) was then added. The middle layer was a methanol–chloroform mixture (1:10, 10 ml), which was covered by a layer of methanol (10 ml), to which 100 µl of NEt_3 was added dropwise. The tube was sealed, and black plate-like single crystals appeared within 3-4 weeks (yield *ca* 75%). Elemental analysis calculated for $C_{38}H_{38}FeN_{12}O_2$: C, 60.80; H, 5.10; N, 22.39. Found: C, 60.50; H, 5.31; N, 22.71.

8. Refinement

Crystal data, data collection and structure refinement details are summarized in Table 3. H atoms were placed in calculated positions using idealized geometries, with C—H = 0.98 Å for methyl groups and 0.95 Å for aromatic H atoms, and refined using a riding model with U_{iso}(H) = 1.2–1.5U_{eq}(C); the hydrogen atom H26 was refined freely. Two OMIT commands were used to exclude beamstop-affected data.

Acknowledgements

Author contributions are as follows: Conceptualization, KZ and MS; methodology, KZ; formal analysis, IOF; synthesis, SOM; single-crystal measurements, S*S*; writing (original draft), MS; writing (review and editing of the manuscript), TYS, MS; visualization and calculations, VMA; funding acquisition, KZ, MS.

Funding information

Funding for this research was provided by a grant from the Ministry of Education and Science of Ukraine for perspective development of a scientific direction 'Mathematical sciences and natural sciences' at Taras Shevchenko National University of Kyiv.

References

Bartual-Murgui, C., Piñeiro-López, L., Valverde-Muñoz, F. J., Muñoz, M. C., Seredyuk, M. & Real, J. A. (2017). *Inorg. Chem.* **56**, 13535–13546.
Bonhommeau, S., Lacroix, P. G., Talaga, D., Bousseksou, A., Seredyuk, M., Fritsky, I. O. & Rodriguez, V. (2012). *J. Phys. Chem. C*, **116**, 11251–11255.
Chang, H. R., McCusker, J. K., Toftlund, H., Wilson, S. R., Trautwein, A. X., Winkler, H. & Hendrickson, D. N. (1990). *J. Am. Chem. Soc.* **112**, 6814–6827.
Dolomanov, O. V., Bourhis, L. J., Gildea, R. J., Howard, J. A. K. & Puschmann, H. (2009). *J. Appl. Cryst.* **42**, 339–341.
Drew, M. G. B., Harding, C. J., McKee, V., Morgan, G. G. & Nelson, J. (1995). *J. Chem. Soc. Chem. Commun.* pp. 1035–1038.
Groom, C. R., Bruno, I. J., Lightfoot, M. P. & Ward, S. C. (2016). *Acta Cryst.* B**72**, 171–179.
Gütlich, P. & Goodwin, H. A. (2004). *Top. Curr. Chem.* **233**, 1–47.
Halcrow, M. A. (2014). *New J. Chem.* **38**, 1868–1882.
Halcrow, M. A., Capel Berdiell, I., Pask, C. M. & Kulmaczewski, R. (2019). *Inorg. Chem.* **58**, 9811–9821.
Kershaw Cook, L. J., Mohammed, R., Sherborne, G., Roberts, T. D., Alvarez, S. & Halcrow, M. A. (2015). *Coord. Chem. Rev.* **289–290**, 2–12.
Macrae, C. F., Sovago, I., Cottrell, S. J., Galek, P. T. A., McCabe, P., Pidcock, E., Platings, M., Shields, G. P., Stevens, J. S., Towler, M. & Wood, P. A. (2020). *J. Appl. Cryst.* **53**, 226–235.

Parsons, S., Flack, H. D. & Wagner, T. (2013). *Acta Cryst.* B**69**, 249–259.
Rigaku OD (2022). *CrysAlis PRO*. Rigaku Oxford Diffraction, Yarnton, England.
Schäfer, B., Rajnák, C., Šalitroš, I., Fuhr, O., Klar, D., Schmitz-Antoniak, C., Weschke, E., Wende, H. & Ruben, M. (2013). *Chem. Commun.* **49**, 10986–10988.
Seredyuk, M., Znovjyak, K., Valverde-Muñoz, F. J., da Silva, I., Muñoz, M. C., Moroz, Y. S. & Real, J. A. (2022). *J. Am. Chem. Soc.* **144**, 14297–14309.
Seredyuk, M., Znovjyak, K. O., Kusz, J., Nowak, M., Muñoz, M. C. & Real, J. A. (2014). *Dalton Trans.* **43**, 16387–16394.
Sheldrick, G. M. (2015*a*). *Acta Cryst.* A**71**, 3–8.
Sheldrick, G. M. (2015*b*). *Acta Cryst.* C**71**, 3–8.
Shiga, T., Saiki, R., Akiyama, L., Kumai, R., Natke, D., Renz, F., Cameron, J. M., Newton, G. N. & Oshio, H. (2019). *Angew. Chem. Int. Ed.* **58**, 5658–5662.
Spackman, P. R., Turner, M. J., McKinnon, J. J., Wolff, S. K., Grimwood, D. J., Jayatilaka, D. & Spackman, M. A. (2021). *J. Appl. Cryst.* **54**, 1006–1011.
Valverde-Muñoz, F.-J., Seredyuk, M., Muñoz, M. C., Molnár, G., Bibik, Y. S. & Real, J. A. (2020). *Angew. Chem. Int. Ed.* **59**, 18632–18638.
Zhang, W., Zhao, F., Liu, T., Yuan, M., Wang, Z. M. & Gao, S. (2007). *Inorg. Chem.* **46**, 2541–2555.

supporting information

Acta Cryst. (2022). E**78**, 1107-1112 [https://doi.org/10.1107/S2056989022009744]

Crystal structure of bis{3-(3,4-dimethylphenyl)-5-[6-(1*H*-pyrazol-1-yl)pyridin-2-yl]-4*H*-1,2,4-triazol-4-ido}iron(II) methanol disolvate

Kateryna Znovjyak, Igor O. Fritsky, Tatiana Y. Sliva, Vladimir M. Amirkhanov, Sergey O. Malinkin, Sergiu Shova and Maksym Seredyuk

Computing details

Data collection: *CrysAlis PRO* (Rigaku OD, 2022); cell refinement: *CrysAlis PRO* (Rigaku OD, 2022); data reduction: *CrysAlis PRO* (Rigaku OD, 2022); program(s) used to solve structure: SHELXT (Sheldrick, 2015a); program(s) used to refine structure: *SHELXL2018/3* (Sheldrick, 2015b); molecular graphics: *OLEX2* (Dolomanov *et al.*, 2009); software used to prepare material for publication: *OLEX2* (Dolomanov *et al.*, 2009).

Bis{3-(3,4-dimethylphenyl)-5-[6-(1*H*-pyrazol-1-yl)pyridin-2-yl]-4*H*-1,2,4-triazol-4-ido}iron(II) methanol disolvate

Crystal data

$[Fe(C_{18}H_{15}N_6)_2]\cdot 2CH_4O$
$M_r = 750.65$
Orthorhombic, *Aea*2
$a = 12.6854$ (10) Å
$b = 26.315$ (2) Å
$c = 10.6511$ (7) Å
$V = 3555.5$ (5) Å^3
$Z = 4$
$F(000) = 1568$
$D_x = 1.402$ Mg m^{-3}
Mo $K\alpha$ radiation, $\lambda = 0.71073$ Å
Cell parameters from 1363 reflections
$\theta = 2.6$–22.8°
$\mu = 0.48$ mm^{-1}
$T = 180$ K
Plate, clear dark red
0.3 × 0.24 × 0.04 mm

Data collection

Xcalibur, Eos diffractometer
Radiation source: fine-focus sealed X-ray tube, Enhance (Mo) X-ray Source
Graphite monochromator
Detector resolution: 16.1593 pixels mm^{-1}
ω scans
Absorption correction: multi-scan (CrysAlisPro; Rigaku OD, 2022)
$T_{min} = 0.824$, $T_{max} = 1.000$
6911 measured reflections
3047 independent reflections
2211 reflections with $I > 2\sigma(I)$
$R_{int} = 0.071$
$\theta_{max} = 25.0°$, $\theta_{min} = 2.2°$
$h = -12\rightarrow15$
$k = -25\rightarrow31$
$l = -12\rightarrow12$

Refinement

Refinement on F^2
Least-squares matrix: full
$R[F^2 > 2\sigma(F^2)] = 0.061$
$wR(F^2) = 0.100$
$S = 1.00$
3047 reflections
247 parameters
1 restraint
Primary atom site location: dual
Hydrogen site location: mixed
H atoms treated by a mixture of independent and constrained refinement

$w = 1/[\sigma^2(F_o^2) + (0.0192P)^2]$
where $P = (F_o^2 + 2F_c^2)/3$
$(\Delta/\sigma)_{max} < 0.001$
$\Delta\rho_{max} = 0.84$ e Å^{-3}
$\Delta\rho_{min} = -0.50$ e Å^{-3}

Absolute structure: Flack *x* determined using 703 quotients $[(I^+)-(I^-)]/[(I^+)+(I^-)]$ (Parsons *et al.*, 2013).
Absolute structure parameter: −0.02 (3)

Special details

Geometry. All esds (except the esd in the dihedral angle between two l.s. planes) are estimated using the full covariance matrix. The cell esds are taken into account individually in the estimation of esds in distances, angles and torsion angles; correlations between esds in cell parameters are only used when they are defined by crystal symmetry. An approximate (isotropic) treatment of cell esds is used for estimating esds involving l.s. planes.

Fractional atomic coordinates and isotropic or equivalent isotropic displacement parameters (Å²)

	x	*y*	*z*	U_{iso}*/U_{eq}
Fe1	0.500000	0.500000	0.32399 (13)	0.0198 (3)
N13	0.3533 (4)	0.48261 (19)	0.3181 (6)	0.0170 (12)
N23	0.4520 (4)	0.5467 (2)	0.1903 (5)	0.0202 (15)
N19	0.3481 (4)	0.5393 (2)	0.1587 (4)	0.0219 (15)
N10	0.4953 (5)	0.4455 (3)	0.4514 (5)	0.0211 (15)
O26	0.1937 (5)	0.3536 (3)	0.6135 (7)	0.074 (3)
H26	0.255 (9)	0.359 (4)	0.602 (8)	0.10 (4)*
N12	0.3978 (4)	0.3867 (2)	0.5544 (4)	0.0214 (15)
N9	0.5624 (4)	0.4206 (2)	0.5293 (5)	0.0205 (15)
C14	0.2907 (5)	0.5053 (3)	0.2340 (6)	0.0189 (17)
C16	0.1439 (5)	0.4588 (3)	0.3039 (6)	0.0266 (18)
H16	0.070880	0.450760	0.300859	0.032*
C11	0.3991 (6)	0.4244 (3)	0.4689 (6)	0.0187 (17)
C18	0.3142 (5)	0.4458 (3)	0.3926 (6)	0.0208 (17)
C17	0.2084 (5)	0.4332 (3)	0.3877 (6)	0.0232 (18)
H17	0.180469	0.407444	0.440732	0.028*
C2	0.5444 (6)	0.3525 (3)	0.6874 (6)	0.0221 (17)
C15	0.1835 (5)	0.4957 (3)	0.2245 (5)	0.0231 (17)
H15	0.139860	0.513428	0.166841	0.028*
C20	0.3249 (6)	0.5650 (3)	0.0514 (6)	0.028 (2)
H20	0.258538	0.565681	0.010235	0.034*
C7	0.6517 (6)	0.3493 (3)	0.7117 (6)	0.031 (2)
H7	0.698294	0.368889	0.661329	0.037*
C21	0.4130 (6)	0.5893 (3)	0.0140 (7)	0.031 (2)
H21	0.420863	0.610314	−0.057996	0.038*
C6	0.6947 (6)	0.3191 (3)	0.8056 (7)	0.0300 (19)
C5	0.6260 (7)	0.2904 (3)	0.8814 (7)	0.036 (2)
C4	0.5194 (7)	0.2928 (3)	0.8593 (6)	0.040 (2)
H4	0.473076	0.273418	0.910428	0.048*
C22	0.4901 (6)	0.5776 (3)	0.1021 (7)	0.0274 (19)
H22	0.560432	0.589870	0.099718	0.033*
C24	0.8132 (5)	0.3196 (3)	0.8284 (8)	0.048 (2)
H24A	0.846198	0.345213	0.774413	0.072*
H24B	0.842489	0.286043	0.808838	0.072*

H24C	0.827202	0.327787	0.916573	0.072*
C8	0.5027 (5)	0.3860 (3)	0.5907 (6)	0.0205 (17)
C3	0.4769 (6)	0.3232 (3)	0.7632 (6)	0.035 (2)
H3	0.402940	0.323876	0.749434	0.042*
C27	0.1677 (7)	0.3185 (4)	0.7045 (8)	0.060 (3)
H27A	0.208643	0.287319	0.691455	0.089*
H27B	0.092312	0.310638	0.699199	0.089*
H27C	0.183692	0.332462	0.787647	0.089*
C25	0.6686 (7)	0.2584 (3)	0.9889 (7)	0.057 (3)
H25A	0.722244	0.234986	0.956909	0.085*
H25B	0.610868	0.238992	1.026777	0.085*
H25C	0.700073	0.280733	1.052319	0.085*

Atomic displacement parameters (Å²)

	U^{11}	U^{22}	U^{33}	U^{12}	U^{13}	U^{23}
Fe1	0.0140 (7)	0.0239 (8)	0.0216 (6)	−0.0013 (8)	0.000	0.000
N13	0.010 (3)	0.020 (3)	0.022 (3)	0.000 (3)	−0.003 (3)	0.002 (3)
N23	0.014 (3)	0.028 (4)	0.019 (3)	−0.003 (3)	0.000 (3)	−0.002 (3)
N19	0.016 (3)	0.024 (4)	0.025 (3)	−0.002 (3)	−0.002 (3)	0.002 (3)
N10	0.019 (3)	0.026 (4)	0.018 (3)	0.001 (3)	−0.003 (3)	0.002 (3)
O26	0.024 (4)	0.082 (6)	0.115 (6)	0.009 (4)	0.018 (4)	0.066 (5)
N12	0.013 (3)	0.025 (4)	0.026 (3)	0.000 (3)	−0.004 (3)	0.001 (3)
N9	0.020 (4)	0.024 (4)	0.018 (3)	0.000 (3)	−0.003 (3)	0.004 (3)
C14	0.012 (4)	0.024 (5)	0.021 (4)	−0.007 (4)	0.003 (3)	−0.003 (3)
C16	0.013 (4)	0.034 (5)	0.032 (5)	−0.005 (4)	0.003 (3)	0.000 (4)
C11	0.022 (4)	0.019 (5)	0.015 (4)	−0.001 (4)	−0.004 (3)	−0.002 (3)
C18	0.014 (4)	0.028 (5)	0.020 (3)	−0.002 (4)	0.002 (3)	−0.004 (3)
C17	0.012 (4)	0.032 (5)	0.025 (4)	−0.009 (4)	−0.002 (3)	0.000 (4)
C2	0.025 (4)	0.024 (5)	0.017 (4)	−0.002 (4)	−0.005 (3)	−0.001 (3)
C15	0.015 (4)	0.027 (5)	0.028 (4)	0.001 (4)	−0.007 (3)	0.004 (4)
C20	0.027 (5)	0.036 (5)	0.022 (4)	0.014 (4)	0.001 (3)	0.004 (4)
C7	0.032 (5)	0.032 (5)	0.027 (5)	0.010 (4)	0.003 (4)	0.001 (4)
C21	0.024 (5)	0.035 (6)	0.035 (5)	0.006 (5)	0.004 (4)	0.017 (4)
C6	0.038 (5)	0.024 (4)	0.028 (4)	0.013 (4)	−0.013 (4)	−0.007 (4)
C5	0.051 (6)	0.028 (5)	0.030 (4)	0.006 (5)	−0.019 (4)	0.001 (4)
C4	0.056 (6)	0.033 (5)	0.031 (6)	−0.017 (5)	−0.006 (4)	0.013 (4)
C22	0.025 (5)	0.029 (5)	0.029 (4)	−0.010 (4)	0.006 (4)	0.006 (4)
C24	0.040 (5)	0.060 (6)	0.045 (4)	0.020 (5)	−0.008 (5)	0.012 (6)
C8	0.017 (4)	0.024 (5)	0.021 (4)	0.002 (4)	0.002 (3)	−0.005 (3)
C3	0.029 (5)	0.044 (6)	0.031 (4)	−0.009 (4)	−0.011 (4)	0.001 (4)
C27	0.043 (6)	0.056 (7)	0.080 (6)	0.008 (6)	0.020 (5)	0.025 (6)
C25	0.080 (8)	0.044 (7)	0.047 (5)	0.002 (6)	−0.024 (5)	0.012 (4)

Geometric parameters (Å, º)

Fe1—N13	1.917 (5)	C2—C8	1.455 (9)
Fe1—N13^{i}	1.917 (5)	C2—C3	1.407 (9)

Fe1—N23^{i}	1.977 (6)	C15—H15	0.9500
Fe1—N23	1.977 (6)	C20—H20	0.9500
Fe1—N10^{i}	1.974 (6)	C20—C21	1.349 (9)
Fe1—N10	1.974 (6)	C7—H7	0.9500
N13—C14	1.338 (8)	C7—C6	1.389 (9)
N13—C18	1.348 (8)	C21—H21	0.9500
N23—N19	1.375 (7)	C21—C22	1.389 (9)
N23—C22	1.333 (9)	C6—C5	1.409 (10)
N19—C14	1.403 (8)	C6—C24	1.522 (9)
N19—C20	1.360 (8)	C5—C4	1.373 (10)
N10—N9	1.358 (8)	C5—C25	1.520 (10)
N10—C11	1.355 (9)	C4—H4	0.9500
O26—H26	0.79 (11)	C4—C3	1.406 (9)
O26—C27	1.380 (9)	C22—H22	0.9500
N12—C11	1.345 (8)	C24—H24A	0.9800
N12—C8	1.386 (8)	C24—H24B	0.9800
N9—C8	1.352 (8)	C24—H24C	0.9800
C14—C15	1.387 (8)	C3—H3	0.9500
C16—H16	0.9500	C27—H27A	0.9800
C16—C17	1.386 (9)	C27—H27B	0.9800
C16—C15	1.383 (9)	C27—H27C	0.9800
C11—C18	1.463 (9)	C25—H25A	0.9800
C18—C17	1.384 (8)	C25—H25B	0.9800
C17—H17	0.9500	C25—H25C	0.9800
C2—C7	1.388 (9)		

N13—Fe1—N13^{i}	176.2 (4)	C14—C15—H15	121.9
N13—Fe1—N23	80.0 (3)	C16—C15—C14	116.2 (6)
N13—Fe1—N23^{i}	97.3 (2)	C16—C15—H15	121.9
N13^{i}—Fe1—N23	97.3 (2)	N19—C20—H20	126.1
N13^{i}—Fe1—N23^{i}	80.0 (3)	C21—C20—N19	107.8 (7)
N13—Fe1—N10	79.6 (3)	C21—C20—H20	126.1
N13—Fe1—N10^{i}	103.0 (2)	C2—C7—H7	118.2
N13^{i}—Fe1—N10^{i}	79.6 (3)	C6—C7—C2	123.7 (7)
N13^{i}—Fe1—N10	103.0 (2)	C6—C7—H7	118.2
N23^{i}—Fe1—N23	87.9 (3)	C20—C21—H21	127.0
N10^{i}—Fe1—N23	93.0 (2)	C20—C21—C22	106.1 (7)
N10—Fe1—N23^{i}	93.0 (2)	C22—C21—H21	127.0
N10^{i}—Fe1—N23^{i}	159.5 (2)	C7—C6—C5	118.4 (7)
N10—Fe1—N23	159.5 (2)	C7—C6—C24	119.9 (7)
N10—Fe1—N10^{i}	93.2 (4)	C5—C6—C24	121.6 (7)
C14—N13—Fe1	119.4 (5)	C6—C5—C25	120.6 (7)
C14—N13—C18	119.8 (6)	C4—C5—C6	119.1 (7)
C18—N13—Fe1	120.6 (5)	C4—C5—C25	120.3 (8)
N19—N23—Fe1	112.5 (4)	C5—C4—H4	119.1
C22—N23—Fe1	140.8 (5)	C5—C4—C3	121.9 (7)
C22—N23—N19	105.2 (6)	C3—C4—H4	119.1
N23—N19—C14	116.6 (5)	N23—C22—C21	110.9 (7)

C20—N19—N23	110.0 (6)	N23—C22—H22	124.5
C20—N19—C14	133.2 (6)	C21—C22—H22	124.5
N9—N10—Fe1	138.8 (5)	C6—C24—H24A	109.5
C11—N10—Fe1	114.9 (5)	C6—C24—H24B	109.5
C11—N10—N9	106.3 (6)	C6—C24—H24C	109.5
C27—O26—H26	117 (7)	H24A—C24—H24B	109.5
C11—N12—C8	100.8 (6)	H24A—C24—H24C	109.5
C8—N9—N10	105.7 (5)	H24B—C24—H24C	109.5
N13—C14—N19	111.0 (6)	N12—C8—C2	123.7 (6)
N13—C14—C15	123.3 (6)	N9—C8—N12	113.2 (6)
C15—C14—N19	125.7 (6)	N9—C8—C2	123.1 (6)
C17—C16—H16	119.3	C2—C3—C4	119.8 (7)
C15—C16—H16	119.3	C2—C3—H3	120.1
C15—C16—C17	121.4 (7)	C4—C3—H3	120.1
N10—C11—C18	115.4 (6)	O26—C27—H27A	109.5
N12—C11—N10	114.0 (6)	O26—C27—H27B	109.5
N12—C11—C18	130.6 (7)	O26—C27—H27C	109.5
N13—C18—C11	109.5 (6)	H27A—C27—H27B	109.5
N13—C18—C17	120.5 (6)	H27A—C27—H27C	109.5
C17—C18—C11	130.0 (7)	H27B—C27—H27C	109.5
C16—C17—H17	120.6	C5—C25—H25A	109.5
C18—C17—C16	118.7 (7)	C5—C25—H25B	109.5
C18—C17—H17	120.6	C5—C25—H25C	109.5
C7—C2—C8	121.7 (6)	H25A—C25—H25B	109.5
C7—C2—C3	117.2 (7)	H25A—C25—H25C	109.5
C3—C2—C8	121.1 (6)	H25B—C25—H25C	109.5

Fe1—N13—C14—N19	1.3 (8)	C11—N12—C8—C2	177.6 (6)
Fe1—N13—C14—C15	−178.9 (5)	C11—C18—C17—C16	−178.4 (6)
Fe1—N13—C18—C11	−0.5 (8)	C18—N13—C14—N19	−174.9 (6)
Fe1—N13—C18—C17	−179.7 (5)	C18—N13—C14—C15	4.9 (10)
Fe1—N23—N19—C14	7.5 (7)	C17—C16—C15—C14	0.0 (10)
Fe1—N23—N19—C20	−168.3 (4)	C2—C7—C6—C5	−0.6 (11)
Fe1—N23—C22—C21	163.0 (6)	C2—C7—C6—C24	−177.8 (7)
Fe1—N10—N9—C8	−178.8 (5)	C15—C16—C17—C18	1.1 (11)
Fe1—N10—C11—N12	178.9 (5)	C20—N19—C14—N13	168.7 (7)
Fe1—N10—C11—C18	−1.0 (8)	C20—N19—C14—C15	−11.1 (12)
N13—C14—C15—C16	−3.1 (10)	C20—C21—C22—N23	0.6 (9)
N13—C18—C17—C16	0.7 (11)	C7—C2—C8—N12	173.2 (6)
N23—N19—C14—N13	−5.8 (8)	C7—C2—C8—N9	−8.5 (11)
N23—N19—C14—C15	174.4 (6)	C7—C2—C3—C4	0.6 (11)
N23—N19—C20—C21	−0.4 (8)	C7—C6—C5—C4	0.5 (11)
N19—N23—C22—C21	−0.8 (8)	C7—C6—C5—C25	−177.4 (7)
N19—C14—C15—C16	176.7 (6)	C6—C5—C4—C3	0.0 (12)
N19—C20—C21—C22	−0.1 (9)	C5—C4—C3—C2	−0.6 (11)
N10—N9—C8—N12	0.9 (8)	C22—N23—N19—C14	176.5 (6)
N10—N9—C8—C2	−177.5 (6)	C22—N23—N19—C20	0.8 (8)
N10—C11—C18—N13	1.0 (8)	C24—C6—C5—C4	177.7 (7)

N10—C11—C18—C17	−179.9 (7)	C24—C6—C5—C25	−0.3 (12)
N12—C11—C18—N13	−178.9 (7)	C8—N12—C11—N10	0.4 (7)
N12—C11—C18—C17	0.2 (13)	C8—N12—C11—C18	−179.8 (7)
N9—N10—C11—N12	0.2 (8)	C8—C2—C7—C6	177.9 (6)
N9—N10—C11—C18	−179.7 (6)	C8—C2—C3—C4	−177.3 (6)
C14—N13—C18—C11	175.7 (6)	C3—C2—C7—C6	0.0 (11)
C14—N13—C18—C17	−3.6 (10)	C3—C2—C8—N12	−8.9 (11)
C14—N19—C20—C21	−175.2 (7)	C3—C2—C8—N9	169.3 (7)
C11—N10—N9—C8	−0.6 (7)	C25—C5—C4—C3	178.0 (7)
C11—N12—C8—N9	−0.8 (7)		

Symmetry code: (i) −*x*+1, −*y*+1, *z*.